PERGAMON

International Journal of Heat and Mass Transfer 44 (2001) 3025–3042

International Journal of HEAT and MASS TRANSFER

www.elsevier.com/locate/ijhmt

Heat transfer of reciprocating helical tube fitted with full circumferential ribs

S.W. Chang *, L.M. Su

Department of Marine Engineering, National Kaohsiung Institute of Marine Technology, Kaohsiung, Taiwan 811, ROC

Received 28 February 2000; received in revised form 2 November 2000

Abstract

This paper describes a detailed experimental investigation of heat transfer in a reciprocating helical tube fitted with full circumferential ribs with particular reference to the design of a piston for a marine propulsive diesel engine. The parametric test matrix involves Reynolds, Dean, pulsating and buoyancy numbers, respectively, in the ranges 4500–7000, 1050–1600, 0.135–0.458 and 0.000325–0.00943 with five different reciprocating frequencies tested, namely 0, 0.83, 1.25, 1.67 and 2 Hz. The manner in which the pulsating force and reciprocating buoyancy interactively affect the local heat transfer along the inner and outer edges of the coils is illustrated using a number of experimentally based observations. The experimental data reconfirm the presence of Dean vortices with attendant relative increase in local heat transfer on the outer surface, even with the agitated flow field caused by ribs under a reciprocating environment. The pulsating force and reciprocating buoyancy have a considerable influence on the heat transfer present due to the modified vortex flow structures in the ribbed coils. An empirical correlation, which is physically consistent, was developed that permits the individual and interactive effects of pulsating force and reciprocating buoyancy on heat transfer in the ribbed coils to be evaluated.

1. Introduction

To minimize fuel consumption in marine power plant has led the thermodynamic optimization of the propulsive diesel engines that use extremely high cylinder pressures and temperatures. As a typical example, a Sulzer RTA 60C engine has a cylinder diameter of 600 mm and each cylinder is capable of delivering 2369 kW in the speed range 91–114 rev/min. Under these conditions, the maximum cycle pressure and temperature are about 155 bar and 1500°C, respectively [1]. Heat transfer augmentation for the internal cooling systems in the components of the combustion chamber become essential in order to cope with the ever-increasing thermal and mechanical loads as a result of thermodynamic optimization. Due to the high effectiveness in heat transfer, helical cooling passages are usually cast in the cylinder wall and head within which coolant flows to convect heat away from these regions [1]. Since the appropriately arranged ribs on cooling surfaces enhance heat transfer, the helical cooling passage fitted with full circumferential ribs could be a feasible solution for further heat transfer augmentation. Because the piston reciprocates, the cooling concept using a ribbed helical passage in the piston cannot be applied confidently before heat transfer in the reciprocating environment has been investigated and evaluated, and this is the focus of the present work.

When a thermal convective system reciprocates, the pulsating and reciprocating buoyancy forces arise simultaneously to modify the fluid motion and heat transfer [2]. Depending on the geometric features of the ribs inside the reciprocating straight ducts [3–5], the various modes of vortices triggered by the ribs are no longer stagnant but are unsteady due to the interactions between rib-induced secondary flows and the periodic reciprocating forces. The strength, spatial location and circulating manner of these rib-induced vortex cells can be temporally varied when the ribbed duct is reciprocated [3–5] or if the flows are subjected to oscillatory or pulsatile secondary flow [6]. Flow visualization results for angled plates submerged in oscillatory flows have

* Corresponding author.

0017-9310/01/$ - see front matter
PII: S0017-9310(00)00352-5

Nomenclature

A	constant coefficients
a	smooth entry length
B	constant coefficients
Bu	buoyancy number $= \beta(T_w - T_f)\omega^2 rd/W_m^2$
C_p	specific heat of coolant (J/kg K)
d	hydraulic diameter of test tube (m)
D	diameter of coil (m)
Dn	Dean number $= Re\sqrt{d/D}$
e	rib height (m)
f_s	axial location dependent coefficients
g_s	axial location dependent coefficients
H	pitch of ribs (m)
k_f	thermal conductivity of fluid (W/m K)
L	land of rib (m)
Nu	reciprocating Nusselt number $= q_f d/(T_w - T_f)k_f$
Nu_0	non-reciprocating Nusselt number
n	constant coefficients
Pu	pulsating number $= \omega r/W_m$
Pr	Prandtl number $= \mu C_p/k_f$
q_f	convective heat flux (W/m^2)
r	reciprocating amplitude (m)
Re	Reynolds number $= W_m d/\upsilon$
T_f	flow bulk temperature (°C)
T_w	wall temperature (°C)
W_m	mean through flow velocity (m/s)
z	axial coordinate (m)
Z	dimensionless axial location (z/d)

Greek symbols

β	thermal expansion coefficient of coolant (K^{-1})
ω	angular velocity of rotating disc creating reciprocating motion (rad/s)
μ	fluid dynamic viscosity (kg/ms)
υ	fluid kinematic viscosity (m^2/s)
ψ_s	unknown functions
φ	unknown functions

Superscripts

I	inner edge of helical tube
O	outer edge of helical tube

Subscript

0	non-reciprocating state

showed the generation of a double pair counter-rotating vortex cells with one attached to the angled plate while the other is shed away from the plate. The detailed growth or shedding process of these vortices depends on the frequency of flow oscillation, the attack angle of the plate and the maximum flow velocity [6]. Along with the reciprocation-induced pulsating flows, which periodically convect cooler or warmer fluids within the duct, the unsteady vortices in the mainstream create periodic local heat transfer variations as a typical reciprocating effect on heat transfer [3–5]. However, when the ribbed helical pipe reciprocates, the unsteady pulsating and reciprocating buoyancy forces will interact with the centrifugally induced secondary flows in a complex manner when the coolant flows in the rib-roughened curved channel. Neither the mechanisms nor characteristics of heat transfer in such reciprocating rib-roughened helical passages have been explored.

A few studies [7–14] have taken into account the effects of the imposition of oscillating and pulsatile pressures on stationary curved pipe flows. Flows around a planar bend with small curvature assuming a high-frequency sinusoidal pressure oscillation could develop a pair of secondary circulations that are additional to the Dean vortices in the inviscid core [7]. For low frequency oscillatory flows in the planar curved pipe, Zalosh and Nelson [8] have showed it to be similar to the low Dean number steady flow. In [9] the imposition of an oscillating pressure wave on the curved pipe flow was shown to have complex influences on both the axial and secondary flows. The growth and decline of secondary circulations in the curved pipe was often accompanied by secondary flow reversals during a pulsation cycle. The secondary flow caused periodic transverse mixing of fluid between the central region and the pipe wall, providing the boundary-layer-like behavior which led to the expected Prandtl number dependency. Heat transfer was insensitive to the pulsation at very small Prandtl numbers, and the Dean number had to be considerably increased before the additional heat transportation associated with the unsteady transverse mixing became strong enough to affect heat transfer. Simon et al. [9] also showed that the time-averaged Nusselt number was most evidently increased at high Prandtl number, high oscillating amplitudes and low frequencies. However, their follow-up report [10] inferred that, as the perturbation analysis might be limited to a solution of the second order, this method might be inappropriate to acquire accurate prediction for such a complicated secondary flow phenomena in a curved tube subjected to oscillatory pressure, especially at low excitation frequency. Thus the result showed in [9] that, for each Dean number, Nusselt number ratios between curved pulsatile and straight pulsatile flows passed through a maximum value at low frequency parameter was negated in [10]. Similarly, the unsteady flows in the helical pipe were quite complicated. Zabielski and Mestel [13] numerically demonstrated that the cross-pipe motion consists of three re-circulating regions, which rotated around the center of the pipe, changing their size and

orientation in time. They numerically showed that Lyne's vortices manifested themselves mainly at the small curvature limit. The considerably increased pulsatile amplitude developed richer secondary flow structures, as the non-linear terms became dominant. For the heat transfer in a helical pipe with pulsatile fully developed turbulent flow, the pulsation considerably increased the instant local and the circumferential time-averaged heat transfer [14]. The temporally varied flow field had a reverse phase angle with respect to the instant heat transfer so that the instant with maximum flow velocity in a pulsatile cycle corresponded to a minimum local heat transfer rate. In the vicinity of outer edge of pipe, locally maximum heat transfer values in opposition to the minimum heat transfer levels at the inner edge were consistently detected [14]. In summary, the previous studies of pulsatile or oscillatory flows in stationary curved pipes have been mostly analytical or numerical and restricted to laminar flows. However, the nature of pulsating or oscillatory flows in stationary ducts is fundamentally different from reciprocating duct flows, especially when the flow regime involves turbulence [2,5]. Therefore, heat transfer modifications may be expected in a reciprocating rib-roughened helical pipe from its stationary state and from the pulsatile flow in a stationary likewise helical pipe.

The present paper presents the results of an experimental investigation that attempts to assess the combined geometry, pulsating and possible buoyancy interaction on the heat transfer mechanism in a reciprocating rib-roughened helical pipe, thus simulating a possible cooling passage in piston. Detailed results of local heat transfer measurements along the inner and outer helix diameters of the ribbed pipe with and without system reciprocation are initially treated. It is followed by a parametric investigation of the coupled and individual effects of pulsating and reciprocating buoyancy forces on heat transfer with the aim to develop the empirical correlation for such complicated heat transfer phenomena. Finally the physically consistent empirical equations proposed are compared with actual measurements.

2. Apparatus

The reciprocating facility used for this investigation was described previously in [2]. For completeness a brief description of the reciprocating facility will be illustrated along with a detailed description of the test section. Fig. 1 shows a schematic of the reciprocating facility and the air flow loop featuring the main components and instrumentation. The air tank (1) that maintains the pressure level between 6 and 8 bar was continuously filled by a compressor (2). Before air flows into the heat transfer test-module (3), it passes through a dryer (4), a

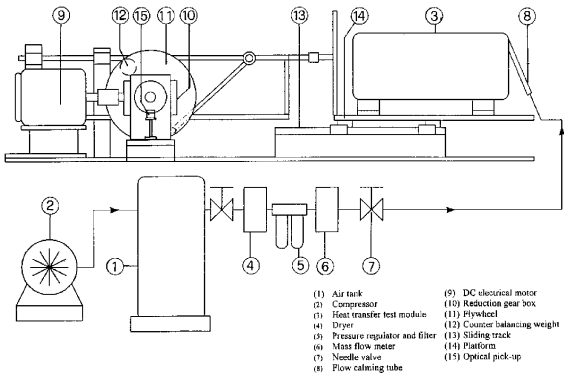

Fig. 1. Reciprocating test facility.

pressure regulator and filter (5), a pressure transducer and Tokyo Keiso TF-1120 mass flowmeter (6) and a needle valve (7). The mass flow rates at the predetermined Reynolds numbers measured at the flow entrance were frequently adjusted to compensate for the variations of fluid properties due to external heating. This was achieved by adjusting the needle valve (7) to retain the variation of Reynolds number within $\pm 0.1\%$. A straight flow calming section (8) with an equivalent length of 20 tube diameter was installed upstream of the coil section. The coolant flow was discharged after it passed through the heated test module (3). System reciprocation was provided by a crank-wheel-mechanism driven by a 2500 W DC motor (9). Through the reduction gearbox (10), the flywheel (11) could be controlled to rotate at any desirable speed measured by the optical pick-up (15). A counter balance weight (12) was fixed on the rotating wheel (11) in order to maintain the dynamic balance during reciprocation. A sliding track (13) was fitted underneath the platform (14) in order to support the heat transfer test module (3).

The test section shown in Fig. 2 was made of a 5260 mm long, 0.5 mm thick stainless steel tube of 20 mm inner tube diameter, with a coil diameter of 264 mm and a pitch of 20 mm. Also depicted in Fig. 2 are the circumferential ribs made by a direct stamping action onto the thin straight tube before it was bent into helix. Due to the deformation of the steel pipe when the die was "clamped" onto the smooth-walled tube, each square rib formed did not have a perfectly sharp edge. The specification of the ribbing geometry has been described in terms of four non-dimensional groups defined in Fig. 2 as

- Smooth entry length/hydraulic diameter ratio $(a/d) = 2.25$.
- Rib height/hydraulic diameter ratio $(e/d) = 0.1$.
- Rib pitch/rib height ratio $(H/e) = 10.0$ and land/pitch ratio $(L/H) = 0.1$.

To generate a reasonably uniform heat flux boundary condition, the test tube was heated directly by passing an electric current through the helical tube. An adjustable

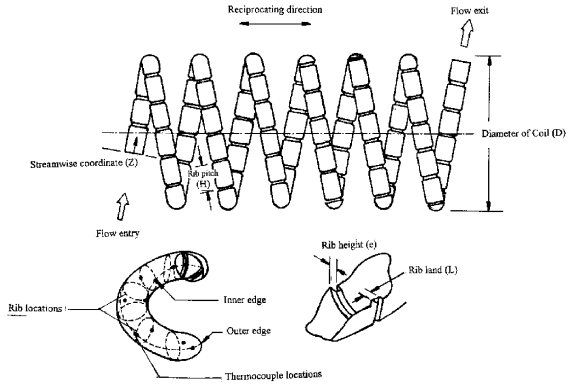

Fig. 2. Test section and the arrangements of ribs and thermocouples.

DC power supply unit that allowed control of the heating power provided the required heating current. Adjusting the heating power supply varies the relative strength of the overall buoyancy level at any fixed flow condition. The complete heated coils were wrapped and insulated with fiberglass. For tests at the highest temperature settings and reciprocating frequency, the estimated heat loss during the experiment was about 9.6% of the total heating power supply. Seventeen K-type thermocouples were mounted along each of the two opposite inner and outer helix diameters of the ribbed coils (Fig. 2). These thermocouples were positioned such that their stream-wise locations corresponded precisely to the rib and mid-rib locations with an interval of 1.5 pitch length between the adjacent thermocouples. Two additional thermocouples were installed into the core of the tube to measure the fluid temperatures at entry and exit planes to the measurement section, and these were used to evaluate the fluid temperature rise. All the temperature measurements were monitored and stored on an IBM PC through a Trend-Link Fluke Hydra data logger for subsequent data processing.

3. Experimental details

The overall experimental apparatus comprises a reciprocating facility onto which the test section as shown in Fig. 2 is attached to reciprocally move with the reciprocating facility. The primary tasks of the present investigation are to generate the heat transfer data in a reciprocating ribbed helical passage and to derive the reciprocating heat transfer correlation. For the particular geometric and thermal boundary conditions simulated, the flow parameters involved in the heat transfer correlation are identified from the dimensionless flow equations. A study of the momentum conservation equations, with the fluid motion referred to a coordinate frame which reciprocates with the flow boundary itself, suggests that the fluid motion is governed parametrically by Reynolds (Re), pulsating (Pu) and reciprocating buoyancy (Bu) numbers [2]. The physical significance of representing the force ratio by each of these dimensionless flow parameters in a reciprocating system has been previously reported [2] while the Dean number (Dn) is customarily defined to characterize the relative strength of the centrifugal force arising in the curved tube. It is thus expected that the local heat transfer on the inner and outer edges of the ribbed test coils, expressed by the local Nusselt number, Nu, will be parametrically described by the following equation

$$Nu = \phi\{Re, Pu, Dn, Bu, Pr, \text{Boundary conditions}\}. \quad (1)$$

All the dimensionless groups appearing in Eq. (1) are defined in the nomenclature section and φ is an, as yet, unknown function. The pulsating number, Pu, and buoyancy number, Bu, respectively, quantify the ratio of pulsating to inertial forces and the relative strength of the reciprocating buoyancy effect [2]. Note that, due to the three-dimensionality of the flow field produced in the reciprocating coiled tube, the unknown function φ in Eq. (1) is dependent on the circumferential and axial locations on the tube surface. In the following, the detailed heat transfer measurements along the inner and outer edges of the test tube will be considered in detail. The I and O superscripts will be adopted to, respectively, refer to these two specific locations in the tube-wise direction.

The experiments were conducted in the Reynolds number range 4500–7000 with reciprocating frequencies at 0, 0.833, 1.25, 1.67 and 2 Hz. The ranges of corresponding Dean and pulsating numbers over which experiments have been performed were 1050–1600 and 0.135–0.458, respectively. By systematically varying the tube wall heat flux, a detailed observation of the buoyancy number effect could be performed. For each Reynolds number, Dean number and reciprocating frequency pair tested, five heater power selections were made to raise the tube wall temperature values to 50°C, 60°C, 80°C, 100°C and 110°C at the axial location of 54 Z. The coolant entry temperature to the test tube was typically in the range 29–40°C and this, in conjunction with the other specified experimental conditions, permitted tests to be undertaken with buoyancy numbers in the range 0.000325–0.00943. Due to the reciprocating effects, the local wall temperature and heat transfer rates were expected to be temporal functions. For each individual test with the particular set of flow parameters, the instantaneous wall temperature measurements for a period of 5 s were averaged and compared with a few following time-averaged temperature scans in order to ensure that the flow condition had reached an equilibrium state. When these time-averaged temperature levels remained within ±0.5°C, the temperature data collected

within the five-second span were stored. These temperature data were subsequently used with other required measurements to evaluate the dimensionless groups defined in Eq. (1). In calculating the Nusselt number, the local fluid bulk temperature was used to define the wall-to-fluid temperature difference. However, due to the difficulty of measuring fluid bulk temperatures inside the test tube without disturbing the flow field, these fluid temperatures were only measured at the flow entrance and exit plane. The intermediate values of fluid bulk temperatures were determined by means of a sequential integration of the local enthalpy balance starting from the location where heating was initiated. Therefore, having the measured flow entry temperature defined as the starting reference, the local fluid bulk temperatures corresponding to the thermocouple positions for wall temperature measurements were accordingly built up. The differences between the calculated exit flow bulk temperatures and measurements were within ±6%. The local coolant properties such as ρ, C_p, k_f, and μ were then defined by means of standard polynomial functions with fluid temperature as the determinant variable. These local properties were incorporated with other measurements such as the coolant mass flow rate and reciprocating frequency to calculate all the dimensionless groups in Eq. (1).

An uncertainty approximation of the data reduction was conducted according to the procedures in [15]. Among all the measurements, one of the major sources to attribute uncertainty was the temperature measurement. As the equilibrium state of the flow system was achieved when the locally time-averaged wall temperature variations were in the range of ±0.5°C with respect to the stable level, the maximum uncertainty in temperature measurement was estimated to be ±0.5°C. With the temperature difference between wall and fluid varying from 23°C to 68°C, the maximum uncertainty for Nusselt, Reynolds, Dean, pulsating and buoyancy numbers were about 16%, 4.7%, 5.1%, 1.2% and 4.2%, respectively.

4. Results and discussion

4.1. General observations

A series of experimental tests with zero reciprocation were undertaken to provide a reference database against which the effect of system reciprocation could be compared and assessed. Fig. 3 illustrates the typical axial Nusselt number distributions along the inner and outer edges for different Reynolds and Dean numbers. It is worth noting that, because the helical pipe is oriented horizontally in order to perform the subsequent parallel-mode reciprocating tests, the vector angle between the mainstream inertial and gravitational forces varies

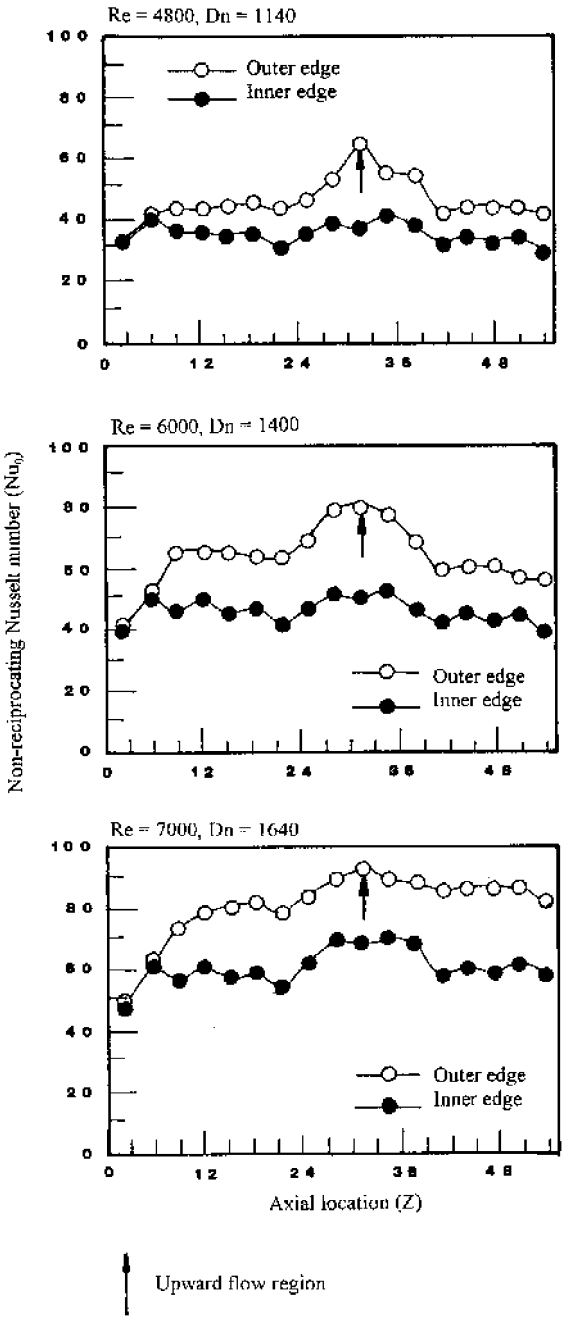

Fig. 3. Typical axial distribution of non-reciprocating Nusselt number.

periodically with, respectively, decelerating and accelerating effects in the upward and downward flow regions. For all the Dean numbers tested it was typical that the heat transfer differences between inner and outer edges gradually developed from the flow entrance, indicating the gradual development of Dean vortices. Excepting the entry flow region where boundary layers

and Dean vortices are initiated, the better cooling effectiveness was consistently found on the outer surface near which the cooler coolant in the flow-core was driven toward the outer edge by the centrifugal force. As shown in Fig. 3 when the Dean number is systematically increased which enhances the relative strength of the Dean vortices, the heat transfer difference between the inner and outer surfaces correspondingly increased. Also along both inner and outer edges, there are local Nusselt number peaks that appear in the upward flow regions of the first coil for all the different Reynolds numbers. Thus the decelerating effect provided by gravity in the upward flow region may moderate the radial velocity distribution which leads to heat transfer increment relative to the downward flow region [14]. In addition to the curvature-attributed influences described above, the rib effects create saw-tooth-like stream-wise heat transfer variations with relatively higher Nusselt number values appearing at the mid-rib locations. Although the rib effects were observed in particular when the flow approached the developed regime, the overall heat transfer phenomena in this stationary ribbed helical pipe mostly followed the typical heat transfer results in the smooth-walled helical pipes within which the Dean vortices are the dominant flow features [14,16]. Hence the present rib design did not qualitatively alter the fundamental heat transfer characteristics in this stationary ribbed helical pipe. It was also noted that the variations of heater power resulted in a relatively thin data band on the local Nusselt number. This implies that the gravity-driven buoyancy did not affect the non-reciprocating heat transfer significantly within the parameter range tested.

The experimental correlations of local Nusselt number data, involving the developing flow and rib effects are axial and circumferential location dependent as illustrated in Fig. 3. Because there was neither significant change in the coolant Prandtl number nor noticeable buoyancy effects for the range of temperatures covered by the experimental program, the local non-reciprocating heat transfer correlations for the inner and outer edges were simplified into functions of Dean number and axial location. For the entire combinations of Dean numbers and heat flux levels tested, having the slight variation in coolant Prandtl number with maximum variation in the range of 1.05% has been absorbed into the numerical coefficients of the correlations that were derived in the form of

$$Nu_0^{\mathrm{I,O}} = A(Z) \times Dn^{B(Z)}. \tag{2}$$

Coefficients A and B are functions of axial location, Z, reflecting the developing nature of the flow with regard to boundary layer, Dean vortices and rib-associated fluid mixing effects. Their variations along the axis of the test pipe are listed in Table 1 and plotted in Fig. 4, respectively.

Over the entire range of Reynolds and Dean numbers and the heat flux levels studied, 92% of the present experimental Nusselt numbers were found to be correlated by Eq. (2) within ±13%. Nevertheless, since the Prandtl number effects were absorbed into the coefficients of Eq. (2) and were not included as a parameter in the correlations that were developed, the results of this study are essentially limited to dry air.

Observation of the axial variations of correlation coefficients A and B could further reveal the effects of

Table 1
Correlative coefficients A and B for stationary Nusselt number, Nu_0

Axial location (Z)	Inner edge		Outer edge	
	Coefficient A	Coefficient B	Coefficient A	Coefficient B
2.267[a]	1.3244	0.4434	2.997	0.3427
5.838	0.7747	0.5617	0.455	0.6757
9.048[a]	0.2253	0.7123	0.10306	0.8507
12.259	0.080	0.8677	0.057665	0.9278
15.469[a]	0.1403	0.7732	0.08845	0.8763
18.681	0.1549	0.7587	0.15673	0.7966
21.676[a]	0.156	0.7438	0.13151	0.8107
25.102	0.1836	0.7409	0.12294	0.8392
28.313[a]	0.4446	0.6284	0.28407	0.7841
31.524	1.0995	0.5002	0.92505	0.5887
34.737[a]	0.6427	0.5780	0.4174	0.6811
37.945	1.4283	0.4568	1.18634	0.5274
41.156[a]	0.8412	0.5114	0.56278	0.6023
44.367	2.0631	0.3916	1.2801	0.4951
47.577[a]	1.0351	0.4850	1.18473	0.5103
50.788	3.7714	0.3087	2.03726	0.4305
53.999[a]	2.4977	0.3515	2.28807	0.4129

[a] Rib location.

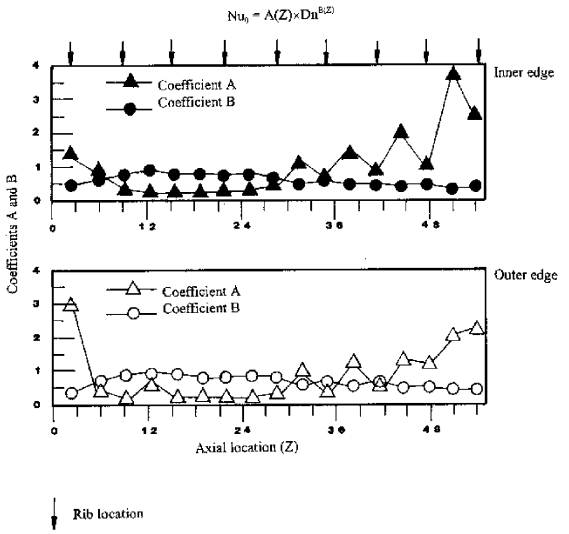

Fig. 4. Axial variation of coefficients A and B.

ribs on heat transfer. As shown in Fig. 4, coefficient A was initially reduced from an entry value for either inner or outer surface. The higher value of coefficient A at the flow entrance is a result of boundary layer development, at which the flow phenomenon was accompanied by a relatively weak inertial force effect so that the lower value of coefficient B was observed for both edges. After about 30 pipe-diameter, the obvious zig-zag axial variation patterns were identified for both coefficients A and B on the inner and outer surfaces. Relatively higher and lower values of coefficients A and B were, respectively, found at the mid-rib and rib locations. Therefore, along with the development of Dean vortices in the coils, secondary rib-flow cells gradually developed to provide an influence on fluid mixing and hence heat transfer. Because the overall trends for coefficients A and B after 30 z/d still show an increasing and descending amplitudes, respectively, as depicted in Fig. 4, the periodic rib-flow cells might not yet be fully developed. For the smooth-walled helical pipe flow, the power index of Dean or Reynolds number in the Nusselt number correlation was normally found to be 0.5. This value is clearly less than 0.8 that is associated with straight turbulent pipe flow [14,16,17]. When the full circumferential ribs were formed in the helical flow passage, the coefficients B at the inner and outer edges for the present ribbed coil were found to be 0.3515 and 0.4129, respectively. Such a reduction from 0.5 could be an indication of a weakened forced convective inertial effect on the heat transfer when the rib-induced flows are gradually established. Accompanying the decay of exponent, B, along the ribbed duct was the corresponding increase in coefficient A. This could be treated as an indication of the heat transfer improvement due to the enhancing fluid mixing in association with rib flows.

Having established the non-reciprocating heat transfer datum and the correlation equations, the comparative difference between the non-reciprocating and reciprocating results can now be examined as follows. A general description of the heat transfer characteristics along the inner and outer edges of the reciprocating helical pipe will be illustrated based on two particular sets of experimental data for Reynolds numbers of 4500 and 5500, respectively, at reciprocating frequencies of 0.833, 1.25, 1.67 and 2 Hz. As shown in Figs. 5(a) and (b) for any fixed Reynolds and Dean numbers, the increase of reciprocating frequency in these two figures caused subsequent increases in pulsating number and therefore increased the relative pulsating to inertial force ratio. Along the outer edge, it was typical to find that the wall temperatures of the reciprocating test coils were temporally varied under the basically uniform heat flux heating condition, which implies the temporal heat transfer variations. The range of such temporal Nusselt number variations at each axial location is indicated as a data bar shown in Figs. 5(a) and (b) with the time-averaged heat transfer level marked. As shown, the most noticeable amplitude of temporal variation of the Nusselt number only appeared at the outer surface, the extend of which increased with the pulsating number. In the upward flow region of the outer surface, the relatively larger data span was measured indicating the evolution of rich time-varied vortex flow structure. Because significant temporal Nusselt number variations were detected on the outer surface, it may be speculated that the flow structures affecting the centrifugal and rib-induced secondary flow cells near the outer edge of the helical pipe underwent considerable temporal variations. Around the pipe center and along the radial flow direction, these vortex flow cells could periodically sway, evolve and oscillate in the reciprocating ribbed coils with their evolution and circulation manners affected by the relative strengths of inertial, pulsating and buoyancy forces. As shown in Fig. 5, the regions with violent temporal vortex variations usually appear as large time-varied oscillatory amplitudes of Nusselt number at which fluid mixing could be accordingly improved leading to local heat transfer peak values. These observations are consistent with the heat transfer data reported for a reciprocating straight duct fitted with 90 degree transverse ribs [4]. In the present case, the temporal Nusselt number variations along the inner surface are not clearly evident.

As shown in Fig. 5(a) when the reciprocating frequency increases from 0.833 to 2 Hz with $Dn = 1070$, the heat transfer difference between the inner and outer edges is gradually reduced. This observation has led to an indication of weakened Dean vortices as a result of enhancing the reciprocating force. Conversely as shown in Fig. 5(b) when the Dean number remains at 1300, the heat transfer difference between the inner and outer

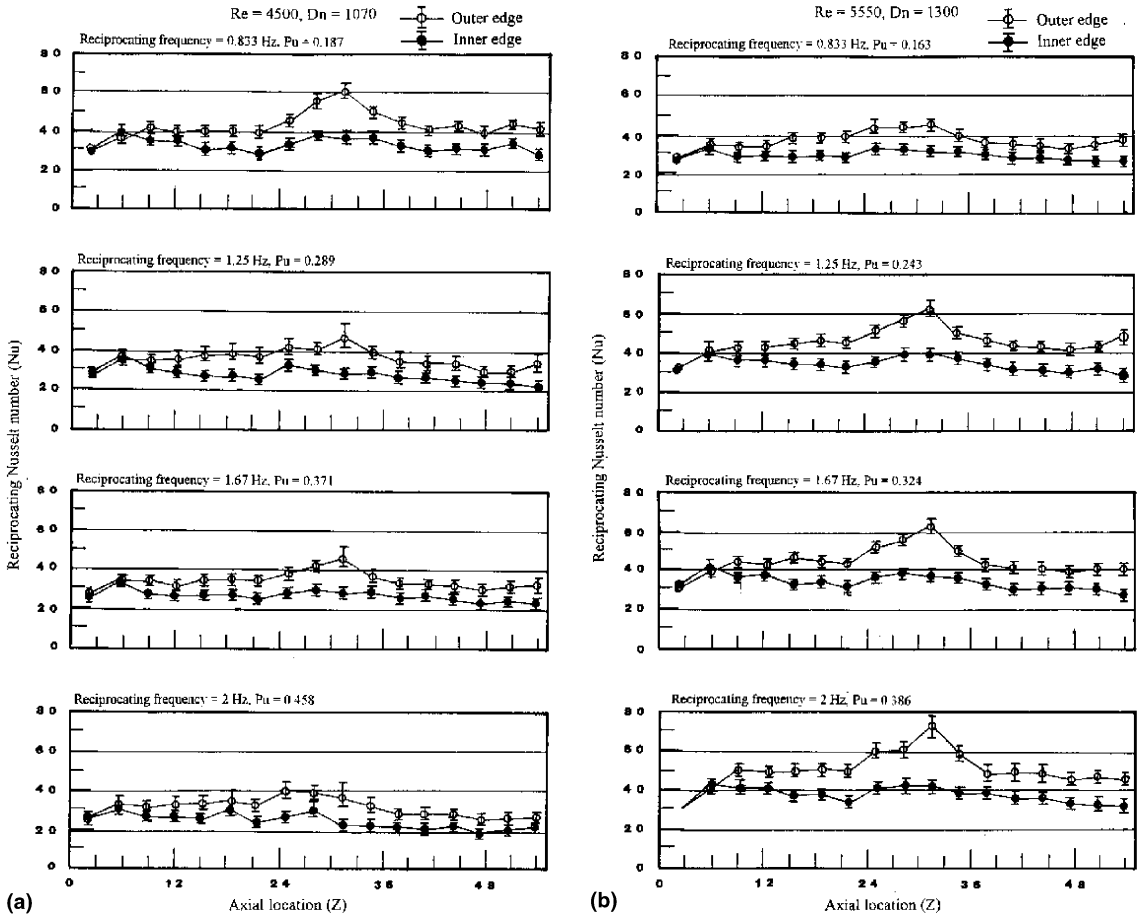

Fig. 5. (a) Typically axial distributions of reciprocating Nusselt number at Dean number of 1070 with pulsating numbers of 0.187, 0.289, 0.371 and 0.458. (b) Typically axial distributions of reciprocating Nusselt number at Dean number of 1300 with pulsating numbers of 0.163, 0.243, 0.324 and 0.386.

edges gradually increases, which implies a strengthening of the Dean vortices due to the enhancement of reciprocating force. Thus when the Dean vortices are weakened, Fig. 5(a) shows the corresponding overall heat transfer reduction when the pulsating number increases from 0.187 to 0.458. However, as shown in Fig. 5(b), where the Dean vortices may be enhanced as a result of increasing the reciprocating force, the overall heat transfer levels are gradually improved and this occurs when the pulsating number increases from 0.163 to 0.386. One speculation to explain the result found in Figs. 5(a) and (b) is the respective cancelling and enhancing effects between rib-induced secondary flow cells in the reciprocating environment with the appearance of Dean's and Lyne's vortices in unsteady curved pipe flow. Thus the pulsating force alone could either impede or enhance heat transfer, whose effect depends on the interactions with centrifugally driven vortices characterized by the other flow parameters listed in Eq. (1). Nevertheless, Figs. 5(a) and (b) indicate different flow interactions when the pulsating number increases. The data showing the temporal Nusselt number variations along the outer edge always increase, indicating that the outer edge undergoes rich variations of secondary flow structures. This particular heat transfer phenomenon does not appear on the inner edge where the temporal Nusselt number variations are usually weak as indicated in Figs. 5(a) and (b). A possible net result occurring at the inner edge could be the moderation of large-scale temporal variations of the vortex cells. As shown in Figs. 5(a) and (b), the cyclical ripples in the axial heat transfer distributions with the relative heat transfer increment in the upward flow region of the inner surface shown in Fig. 3 are considerably suppressed when the ribbed coils reciprocate. Therefore the centrifugal and rib-induced vortex flow cells were experiencing the complicated interactive merging or enhancing process triggered by the periodic pulsating forces. Due to the

various degrees of interactive effects between reciprocating and centrifugal forces with the rib-induced secondary flows, the heat transfer differences between the inner and outer edges at a fixed Dean number could be either increased or decreased with the pulsating number as shown in Fig. 5. In particular, the subsequent influence of weakened Dean vortices on the overall heat transfer performance could sometimes lead to heat transfer reduction from the non-reciprocating situation, which will be illustrated in the following section when the reciprocating and non-reciprocating heat transfer data are compared.

To reveal the reciprocating buoyancy effects on heat transfer, the time-averaged reciprocating Nusselt number data collected at fixed Reynolds, Dean and pulsating numbers with different heating levels are compared. Fig. 6 typifies the axial distributions of time-averaged reciprocating Nusselt numbers along inner and outer edges of the ribbed coils in correspondence with five ascending buoyancy levels for nominal Reynolds number of 4500 at reciprocating frequencies of 0.833, 1.25, 1.67 and 2 Hz. In general, the better heat transfer on the outer edge relative to its inner counterpart was still evident due to the cross-stream Dean vortices, even when both reciprocating forces and rib-induced flows were present. As the buoyancy level increased by increasing the heat flux, the considerable upward data spread of Nusselt number appeared at each measured station for both inner and outer edges which demonstrated the beneficial buoyancy effects on heat transfer. A relatively large data spread, driven by the buoyancy variation was consistently found at the outer edge, reflecting larger buoyancy effect on this surface. Also indicated in each individual plot in Fig. 6 are the equivalent Nusselt number values from a stationary test section obtained at the same Reynolds and Dean numbers. As shown, when the buoyancy number remained at the lower levels, the local Nusselt numbers could be considerably reduced due to system reciprocation. By gradually increasing the buoyancy level at any set of Reynolds, Dean and pulsating numbers, a heat transfer increment due to the increase of buoyancy number was evident. Such a beneficial effect on heat transfer could subsequently lead to relative heat transfer enhancement from the non-reciprocating heat transfer datum.

It is evident that the heat transfer in the reciprocating ribbed helical coils involves a complex interactive mechanism between the force ratios of convective inertial, centrifugal, pulsating and reciprocating buoyancy forces. To further illustrate the individual effects of these force ratios on heat transfer in terms of Reynolds and Dean numbers, the reciprocating Nusselt number, Nu, was scaled relative to the equivalent non-reciprocating Nusselt number level, Nu_0, under conditions with the same Reynolds and Dean numbers. This was achieved by fixing the pulsating and spatially averaged buoyancy numbers while comparing the scaled Nusselt number data, Nu/Nu_0, generated from two different sets of Reynolds and Dean number tests. By using different reciprocating frequencies this shows the individual Reynolds and Dean number effects on reciprocating heat transfer. Fig. 7(a) compares the scaled heat transfer data generated at Reynolds numbers of 4400 and 6800 with the same pulsating number of 0.2. In Fig. 7(a), two pairs of comparisons with the averaged buoyancy numbers of 0.00082 and 0.00121 are illustrated. Similarly, at the same pulsating number of 0.29 with different Reynolds numbers of 4600 and 6400, the scaled Nusselt number data were compared for two different averaged buoyancy numbers of 0.00157 and 0.00263. As shown in Figs. 7(a) and (b), although the pulsating and spatially averaged buoyancy numbers were fixed, the axial distributions of Nusselt number ratios, Nu/Nu_0, generated from two different sets of Reynolds and Dean number tests did not collapse onto a single data band. In general, the lower values of Reynolds and Dean numbers gave higher Nusselt number ratios. This observation indicates the effects that Reynolds or Dean numbers have on heat transfer were modified by the reciprocating forces. In either Fig. 7(a) or Fig. 7(b), the higher the averaged buoyancy numbers were, the higher the Nusselt number ratios appeared. By increasing the buoyancy number from 0.00157 to 0.00263 as shown in Fig. 7(b), the Nusselt number ratios, Nu/Nu_0, could be increased from values of less than 1.0 to levels greater than 1.0. The results shown in Figs. 6 and 7 suggest that the role of reciprocating buoyancy force for the heat transfer modifications in the reciprocating ribbed helical coils is significant.

4.2. Parametrical presentations of heat transfer on inner and outer edges

Figs. 6 and 7 demonstrated the strong interactive effect between convective inertial, centrifugal, pulsating and reciprocating buoyancy forces. As illustrative examples to reveal the overall coupling effect of pulsating and buoyancy force ratios on heat transfer, Fig. 8 shows the plots of scaled Nusselt number ratios, Nu/Nu_0, against buoyancy number, Bu, for all the axial locations measured along the inner and outer edges. As shown, there is a tendency for all the data to collapse onto a data band for both edges with data spread driven by the changes of pulsating and Dean numbers. Also the heat transfer modifications made by the reciprocating forces gradually appear downstream. Along both edges there is an initial impediment to the relative heat transfer with subsequent recovery when the buoyancy number increases. With the presence of reciprocating buoyancy effects, the reciprocating heat transfer could be reduced to about 62% of the equivalent non-reciprocating Nusselt number value when the

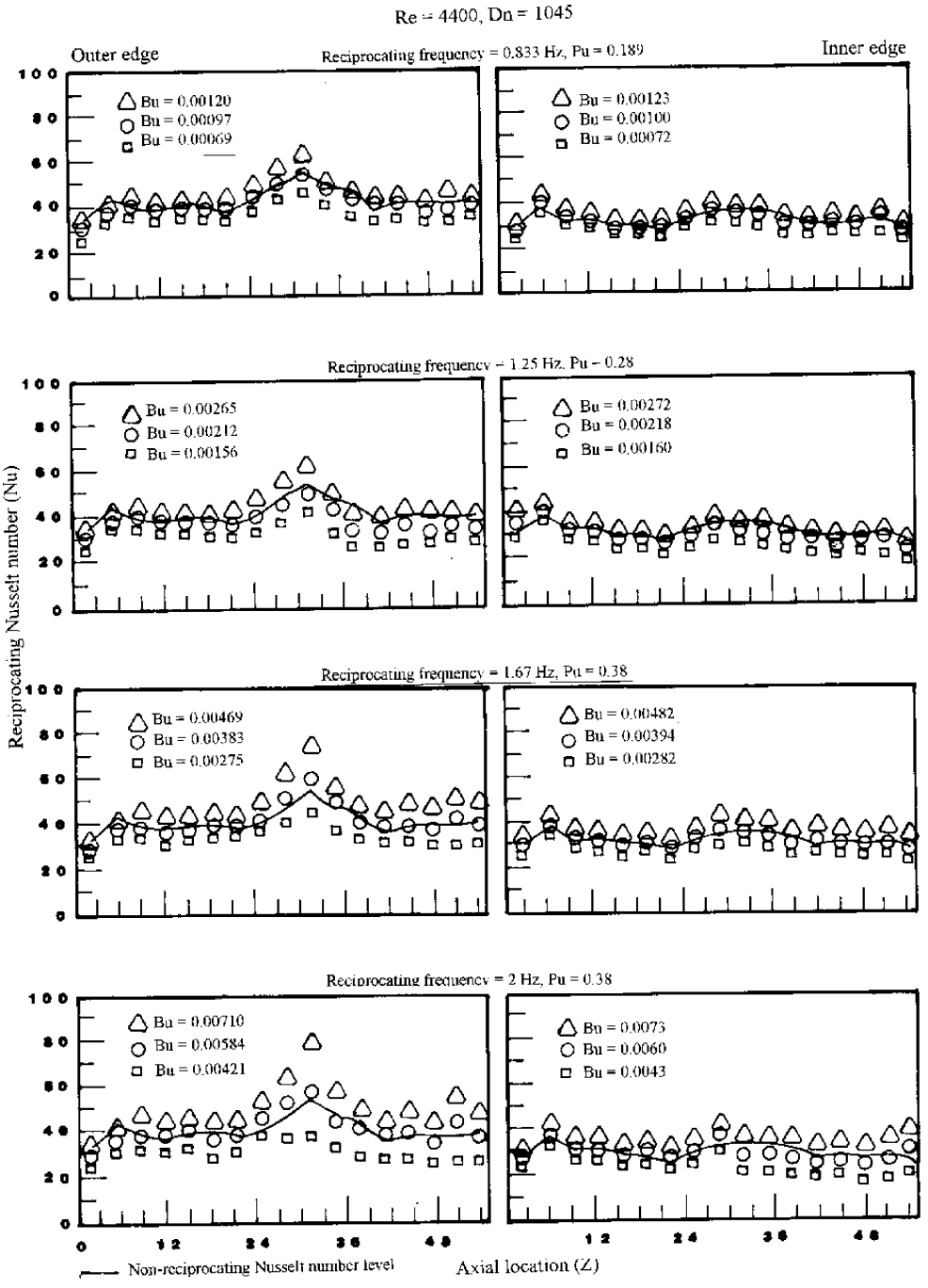

Fig. 6. Axial distributions of reciprocating, Nusselt number with various buoyancy levels.

ribbed helical coils reciprocate. The coupling of individual effects between pulsating and reciprocating buoyancy forces is further illustrated in Fig. 9. As shown in Fig. 9, the existence of such coupling effects between pulsating and reciprocating buoyancy forces is demonstrated when the variations of Nusselt number ratios, Nu/Nu_0, driven by the change in buoyancy number at fixed pulsating numbers are compared. For the heat transfer data at each pulsating number comprises five data points with ascending buoyancy level, $(\beta T_w - T_f)$. This shows a linear-like increase of the scaled reciprocating Nusselt number as the buoyancy

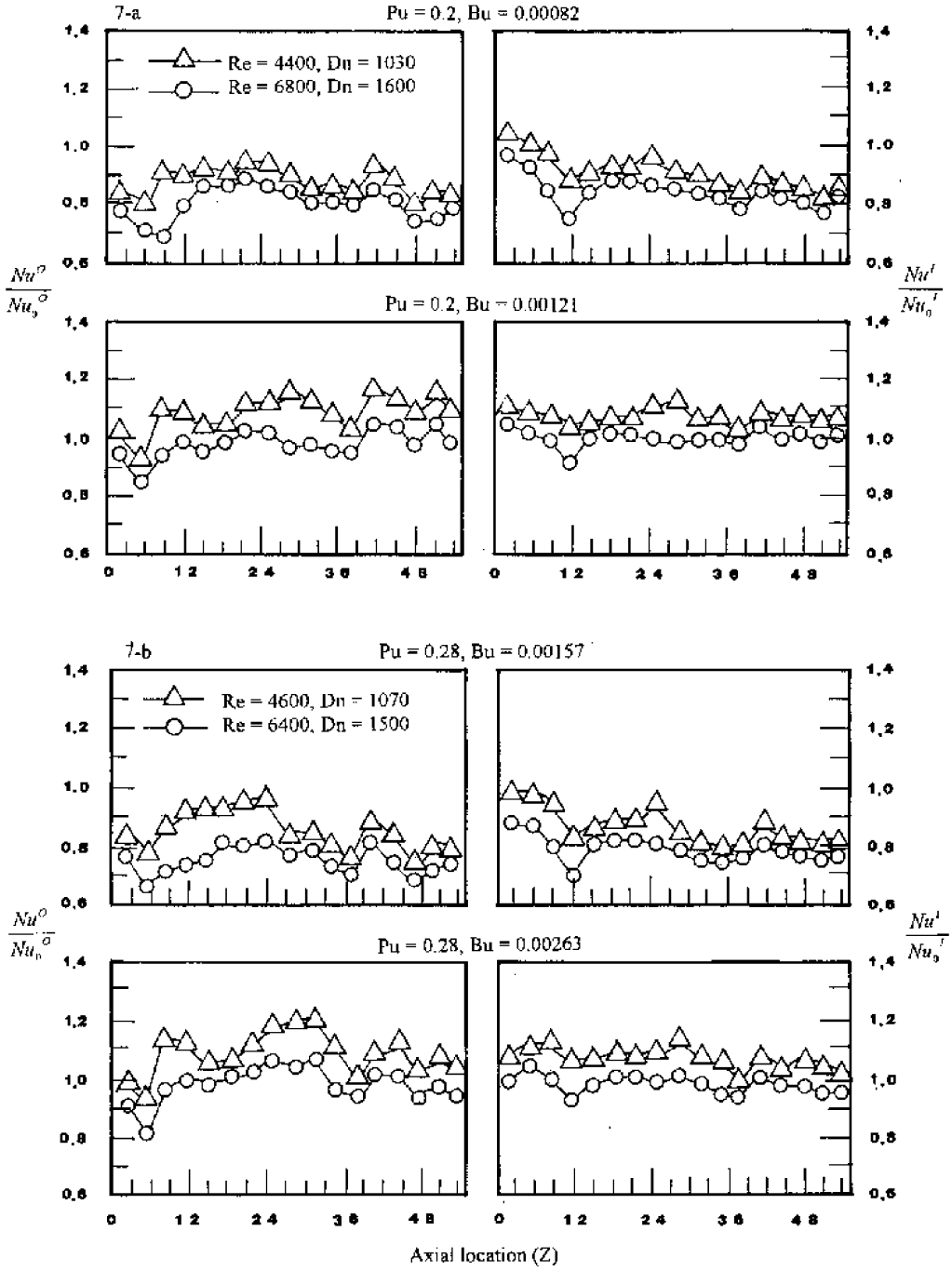

Fig. 7. Axial distribution of normalized Nusselt number at pulsating number values of 0.2 and 0.28.

number is increased. However, to preserve the physical consistency, the coupling noted between the pulsating and buoyancy numbers shown in Fig. 9 must be such that as the buoyancy number becomes zero (by eliminating the wall-to-fluid temperature difference), the reciprocating Nusselt number must still be affected by the pulsating number. The zero buoyancy case applies for example to the analogy of mass transfer from the wall to the fluid in these reciprocating ribbed helical coils. In this case pulsating and centrifugal force driven secondary flows and their related phenomena will still alter the mass transfer even in the absence of buoyancy. Such

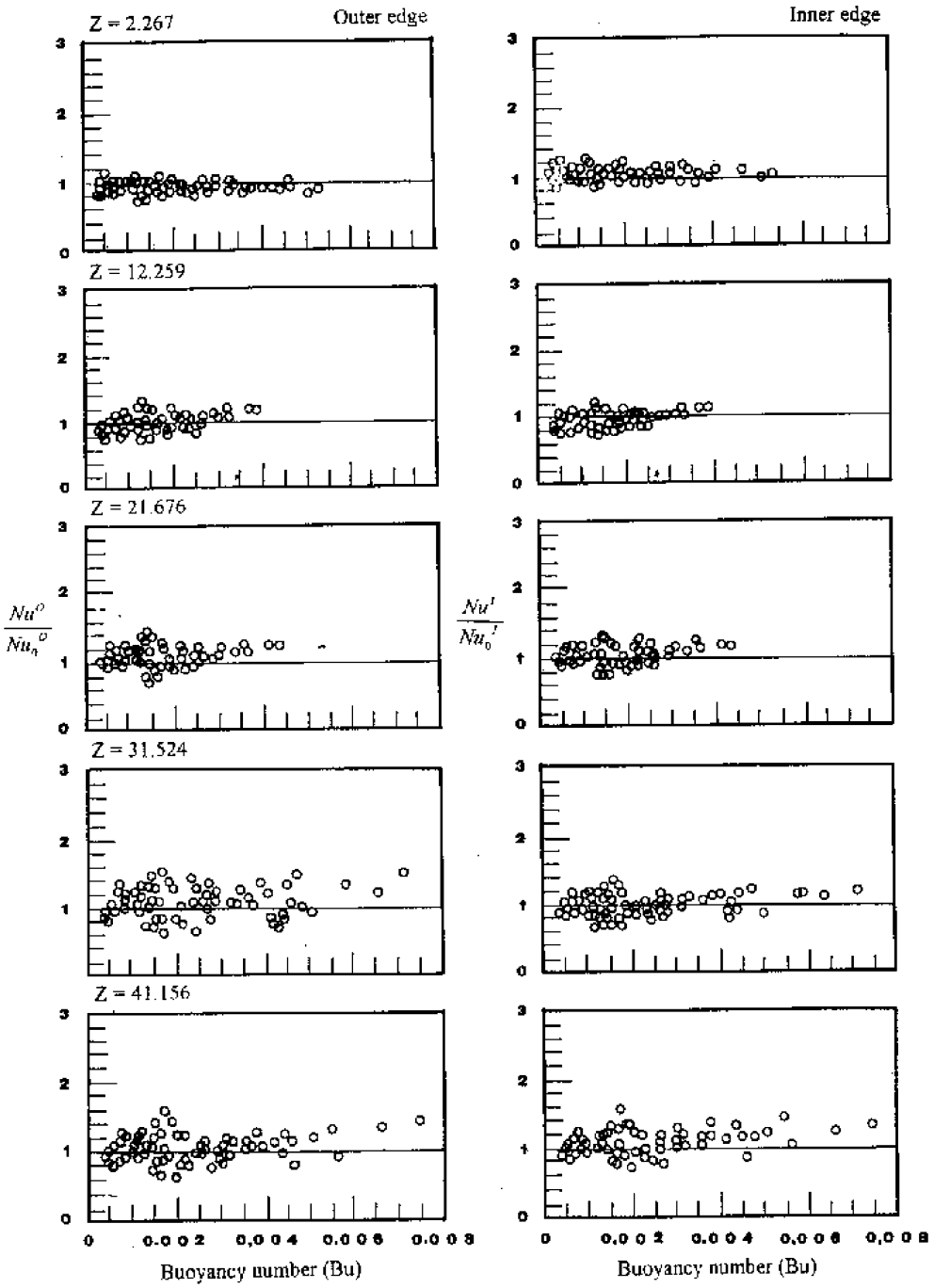

Fig. 8. Effects of reciprocation on local heat transfer of inner and outer edges.

zero buoyancy scenarios are not strictly possible in practice since the heat transfer tests require a finite wall-to-fluid temperature differences. Nevertheless, the zero buoyancy pulsating number effect may be inferred by extrapolating the heat transfer data taken at a specified pulsating number to the buoyancy number of zero. Some selective data to illustrate this extrapolating procedure are also depicted in Fig. 9.

In addition to the fact that the Nusselt number ratios, Nu/Nu_0, increase with the buoyancy number for all the fixed pulsating numbers tested, the slopes of the individual correlation curves shown in Fig. 9 tend to be

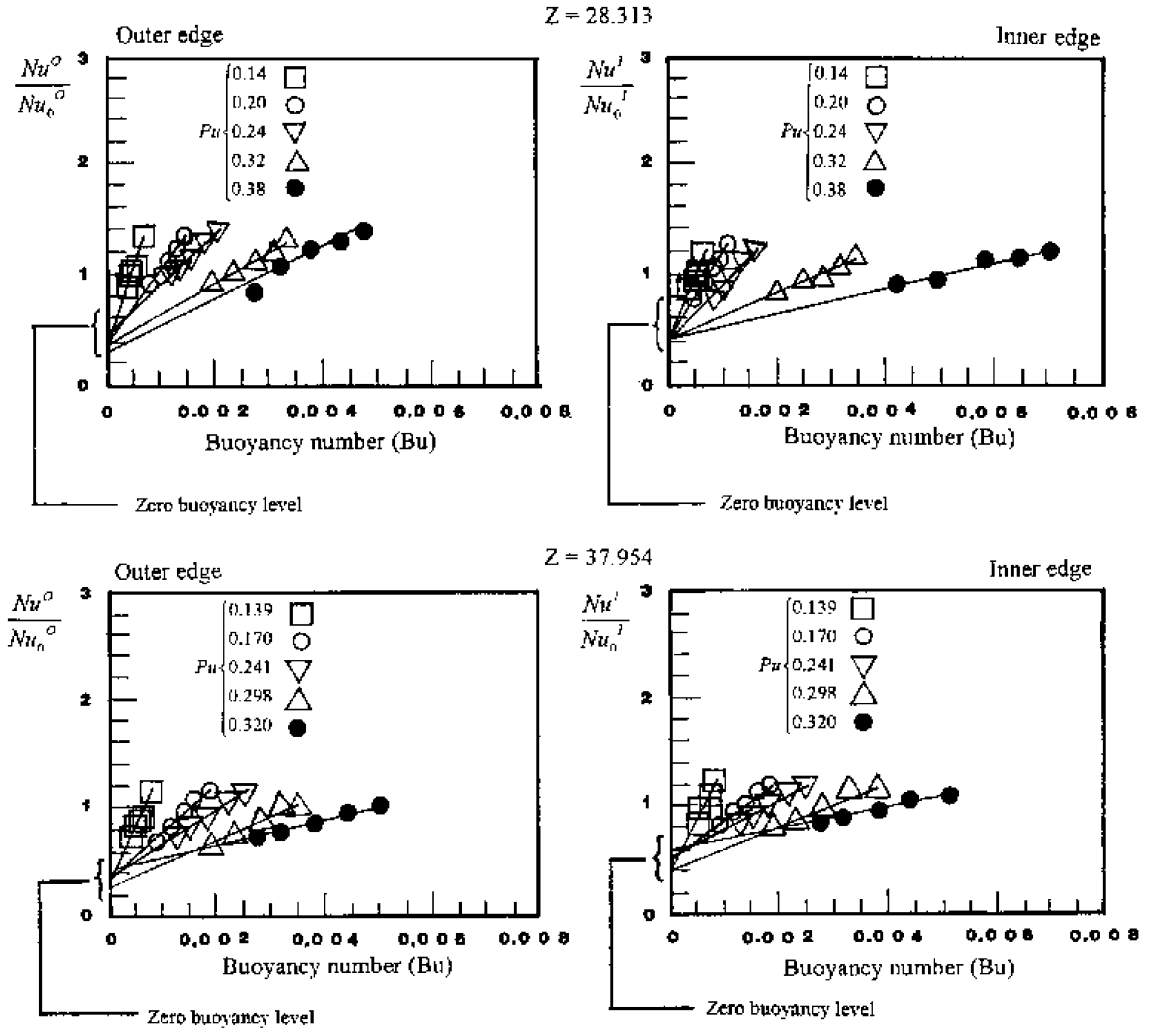

Fig. 9. Extrapolating heat transfer results into zero buoyancy level.

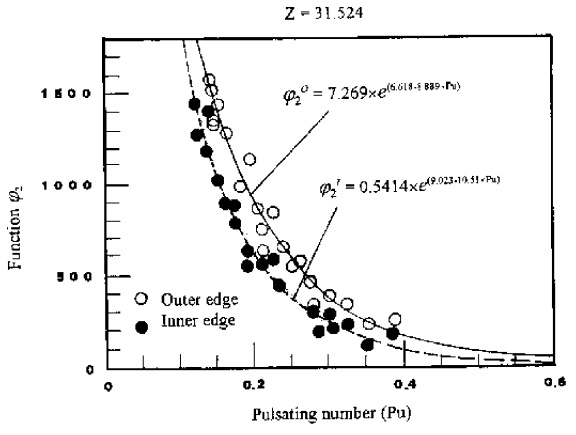

Fig. 10. Variations of function φ_2 at axial location of $Z = 31.524$.

reduced when the pulsating number increases. The physical implication of this slope reduction with increase of pulsating number is the weakened buoyancy effect when the relative strength of the pulsating force is enhanced. Fig. 10 demonstrates the pattern of variation of these slopes against pulsating number along the inner and outer edges at an axial location of $Z = 31.524$. As shown in Fig. 10, the variation in slopes tends to collapse onto a tight data band following the exponential decay. Similar results are observed for the data points collected from all the different axial locations along the coil. Because the patterns of variation for these data show little differences between inner and outer surfaces, it raises the possibility that the coupling between buoyancy and pulsating forces could be isolated from the effects of cross-stream Dean vortices.

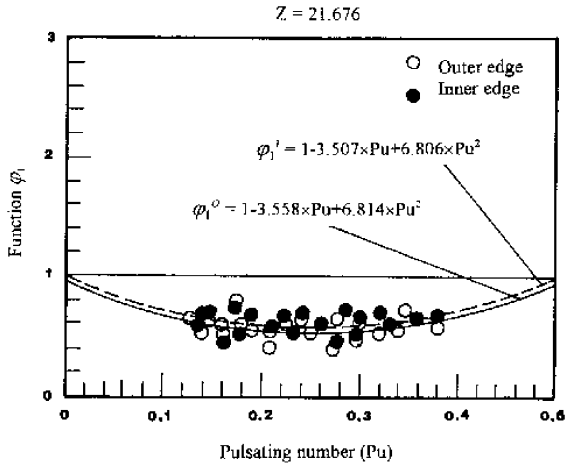

Fig. 11. Variations of function φ_1 at axial location of $Z = 21.676$.

Another important feature revealed in Fig. 9 concerns the precise data values that define the zero-buoyancy Nusselt. As an illustrative example, the extrapolated zero buoyancy results over all the ranges of pulsating numbers for the inner and outer edges at $Z = 21.676$ are shown in Fig. 11. As shown on both inner and outer edges, the most severe heat transfer impediment brought by the pulsating force alone could reduce heat transfer levels to about 53% of the non-reciprocating references at a pulsating number of about 0.24. Thus the weak reciprocation demonstrates the stabilizing effect or the cancellation of vortex strength, leading to significant heat transfer reductions. However, a subsequent heat transfer recovery tendency gradually develops when the pulsating number continuously increases as depicted in Fig. 11.

On completion of the extrapolation procedure, this zero buoyancy heat transfer data were combined with the raw data to provide a reference datum from which the buoyancy interaction initiates. Using these extrapolated data and the measured heat transfer results, but applied to each measured location, it is possible to construct the variation patterns of Nusselt number ratio, Nu/Nu_0, against the pulsating number in Fig. 12 for a range of buoyancy levels. Because the relative strength of the buoyancy force is correspondingly enhanced by the increase of pulsating number (under an approximately similar range of wall-to-fluid temperature differences; $T_w - T_f$), the data spread driven by the variation in buoyancy number shown in Fig. 12 increases with the pulsating number. As the buoyancy interaction within this particular parametric range shows beneficial effects on heat transfer enhancement, the data spread from the zero-buoyancy reference datum is driven upward with the increase of buoyancy number as shown in Fig. 12. Therefore, heat transfer improvement relative to the non-reciprocating data is mainly attributed to the buoyancy interaction.

The general effect of reciprocation on heat transfer in terms of the dimensionless groups shown in Eq. (1) within the test tube has been demonstrated. However, if the interactive effects in association with the Dean number were absorbed into the coefficients in the correlation for assessing the influences of reciprocation on local heat transfer, the simplified version of the correlation could be argued to take the form of

$$\frac{Nu^{I,O}}{Nu_0} = \phi(Pu, Bu, Z). \tag{3}$$

The mathematical structure of the function ϕ in Eq. (3) has to satisfy the following two physical constraints. Firstly, the function ϕ has to be unity when the pulsating number is zero, reflecting the non-reciprocating forced convection solution. Secondly, as the buoyancy number approaches zero there is still a pulsating force driven heat transfer modification, which has been illustrated in Figs. 9 and 12. In Fig. 9, at each axial location with a range of pulsating number values demonstrated that the relative Nusselt number ratio, $Nu^{I,O}/Nu_0$, could be a linear function of the buoyancy number. The lines shown in Fig. 9 are a linear regression of the experimental data and they have been extrapolated to the zero buoyancy level. The evidence depicted in Fig. 9 and the restrictions on the functional form of Eq. (3) have led to the proposal that a possible specific form of the correlation could be

$$\frac{Nu^{I,O}}{Nu_0} = \psi_1(Pu, Z) + \psi_2(Pu, Z)\, Bu, \tag{4}$$

in which ψ_1 and ψ_2 are functions of the pulsating number and the dimensionless axial location. Note that ψ_1 has to be unity at zero pulsating number to meet the first physical constraint cited above. In order to determine the functional shapes of ψ_1 and ψ_2, a series of cross plots based on Fig. 9 but applied to the entire range of axial locations were performed to interpolate a series of curves for $Nu^{I,O}/Nu_0$ against the pulsating number for a range of specified buoyancy levels. Figs. 10 and 11 show typical examples of the manner in which ψ_1 and ψ_2 varied with the pulsating number.

Led by a detailed examination of all the axial location versions of Figs. 10 and 11, it is proposed that ψ_1 and ψ_2 can be reasonably well approximated by the following general forms, which simultaneously satisfy the second constraint.

$$\psi_1 = 1 + f_1(Z)\, Pu + f_2(Z)\, Pu^2, \tag{5}$$

$$\psi_2 = g_1(Z)\, e^{(g_2(Z) - g_3(Z) \times Pu)}, \tag{6}$$

where the f_s and g_s are functions of the non-dimensional axial locations, Z. These structures can be applied to

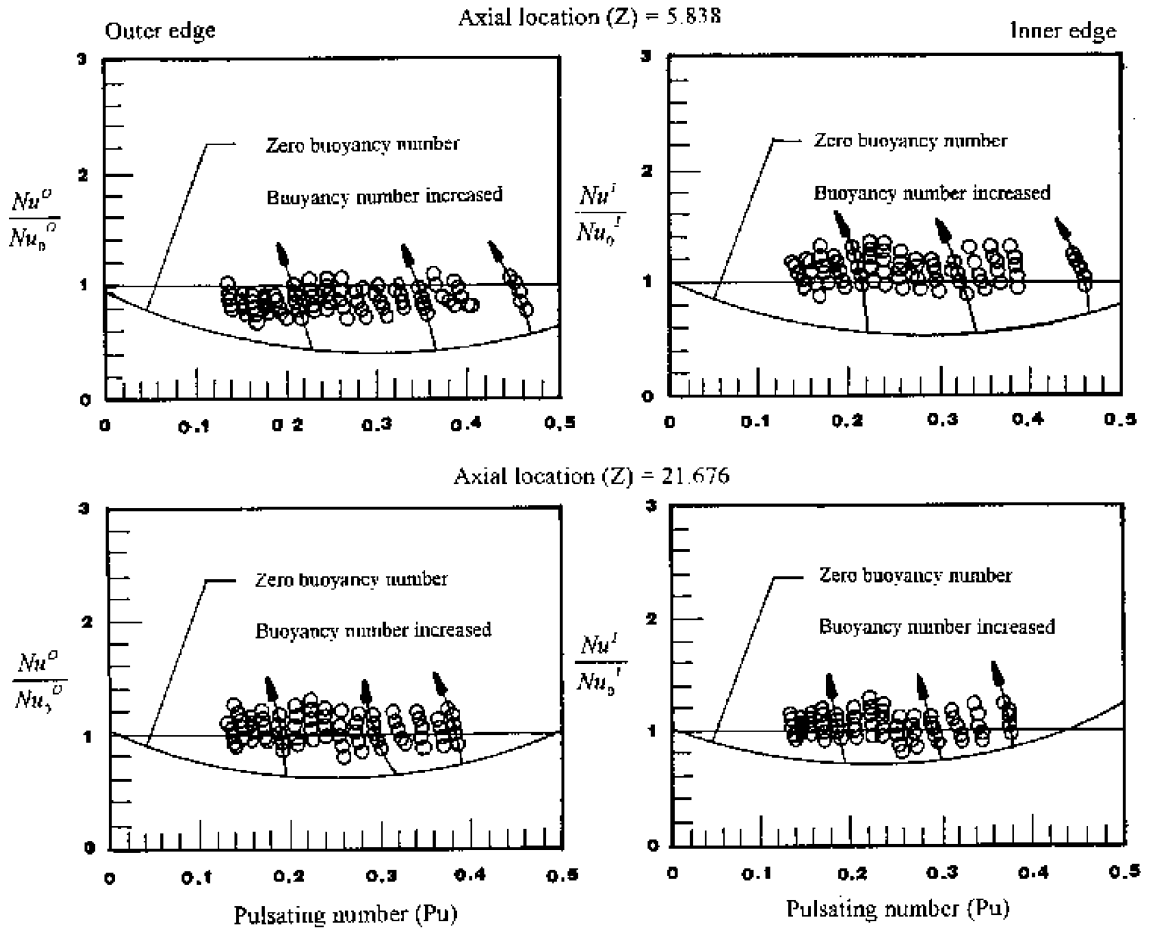

Fig. 12. Variations of extrapolated and experimental heat transfer data with pulsating number.

both inner and outer surfaces but with different f_s and g_s functions. Note that, examining Eq. (5) shows that ψ_1 becomes unity at zero pulsating number, which satisfies the zero reciprocating forced convection limiting case. Tables 2 and 3 list the numerically determined curve fits for the f_s and g_s function values over the inner and outer edges at all the axial locations measured.

The prediction of time-averaged heat transfer in a reciprocating helical tube fitted with full circumferential ribs is a formidable task owing to the complex interaction between the normal forced convection in the coils and the combined influences of pulsating force and reciprocating buoyancy. Fig. 13 compares a selection of the experimental data generated from the present study with the empirical prediction from Eqs. (4)–(6). Over the entire range of experimental data obtained, 88% of the present experimental Nusselt numbers were found to agree within ±20% of the proposed correlation. Considering the overall complexity of this reciprocating situation, the proposed correlation offers a good indication of the likely effects of the combined interaction of pulsating force and reciprocating buoyancy on heat transfer over the inner and outer edges of the ribbed coils. The experimental approach developed in this study for deriving the design friendly correlation based on a physical interpretation of the governing flow equations may be adopted for other reciprocating ducted flow heat transfer problems with different geometries, which could be refined to deal with more sophisticated problems.

5. Conclusions

This experimental study has examined the forced convective heat transfer in a reciprocating helical pipe fitted with periodical full circumferential ribs with particular reference to the heat transfer enhancement of the internal cooling passages of a cooled piston. In conclusion the following observations result from this investigation.

(1) With the presence of a spatially periodic flow field caused by ribs in a stationary helical pipe, the considerable centrifugal effects generate cross-stream Dean

Table 2
Functional values of $f_1(Z)$ and $f_2(Z)$

Axial location (Z)	Inner edge		Outer edge	
	$f_1(Z)$	$f_2(Z)$	$f_1(Z)$	$f_2(Z)$
2.267[a]	−2.404	4.35	−3.73	7.198
5.838	−3.447	7.323	−3.957	7.238
9.064[a]	−2.795	3.041	−3.737	4.687
12.259	−5.617	14.88	−6.54	13.84
15.469[a]	−3.1	4.297	−3.962	7.421
18.681	−3.9	8.072	−3.748	7.06
21.676[a]	−3.507	6.806	−3.558	6.814
25.102	−3.889	8.059	−3.22	4.99
28.313[a]	−3.888	8.056	−4.815	8.677
31.524	−4.856	9.743	−5.941	11.67
34.734[a]	−2.948	3.205	−5.225	10.83
37.945	−2.897	4.368	−3.543	4.538
41.156[a]	−3.2	7.448	−3.322	4.404
44.367	−3.173	4.39	−4.098	4.513
47.577[a]	−2.273	3.028	−4.508	5.855
50.787	−3.389	4.432	−4.532	8.146
53.999[a]	−2.555	1.007	−3.206	4.053

[a] Rib location.

Table 3
Functional values of $g_1(Z)$, $g_2(Z)$ and $g_3(Z)$

Axial location (Z)	Inner edge			Outer edge		
	$g_1(Z)$	$g_2(Z)$	$g_3(Z)$	$g_1(Z)$	$g_2(Z)$	$g_3(Z)$
2.267[a]	3.242	6.472	8.4	0.4377	9.795	14.28
5.838	7.868	6.611	10.95	0.9991	7.545	6.953
9.064[a]	0.6555	8.702	8.161	6.939	6.509	8.703
12.259	4.261	7.834	8.18	6.101	6.322	7.583
15.469[a]	6.101	5.859	6.469	6.286	5.932	6.706
18.681	5.386	6.262	8.461	6.576	5.677	6.284
21.676[a]	0.6039	8.054	7.669	3.1208	0.1015	8.579
25.102	0.3662	8.515	6.614	5.829	6.049	7.172
28.313[a]	0.432	9.356	11.06	5.851	6.536	8.151
31.524	0.5414	9.023	10.51	7.269	6.618	8.887
34.734[a]	0.67	8.428	8.844	6.423	6.615	10.25
37.945	0.1795	10.1	11.96	1.499	6.94	6.373
41.156[a]	0.2306	4.788	9.155	1.257	8.031	9.524
44.367	3.189	6.548	8.389	0.9851	8.2	9.955
47.577[a]	0.7779	8.054	9.029	2.32	8.058	10.96
50.787	3.956	7.326	11.91	5.729	7.018	11.63
53.999[a]	1.7206	8.254	10.89	5.398	5.911	7.445

[a] Rib location.

vortices and result in peripheral heat transfer variation with relative high heat transfer on the outer edge compared with that on the inner edge. A set of experimental correlations was derived for the local non-reciprocating Nusselt number along both the inner and outer edges. The variation patterns of their constitutional coefficients verify the appearance of a spatially periodic heat transfer in the ribbed helical coil after the coolant has traveled about 30 pipe-diameter.

(2) The periodicity of reciprocating forces interacting with centrifugal and rib-associated secondary flows resulted in, respectively, lower and higher temporally oscillatory Nusselt number variations along the inner and outer edges of the reciprocating ribbed helical coils. Considerable heat transfer differences between the inner and outer edges were still evident in the reciprocating ribbed helical coils. Nevertheless, due to the stabilizing effect or vortex flow cancellation caused by weak recip-

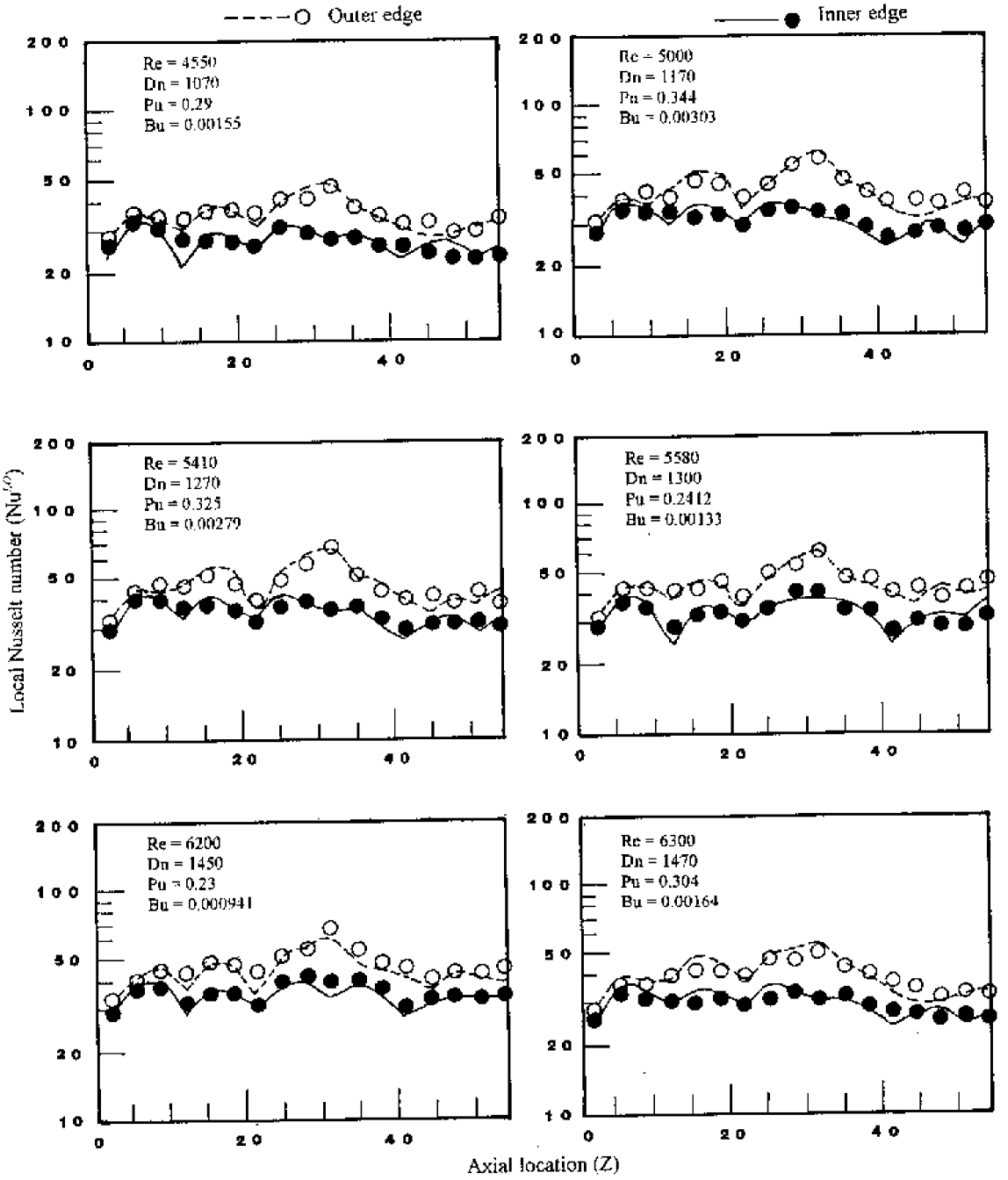

Fig. 13. Comparison of proposed correlations with experimental data points.

rocation, considerable heat transfer impediment from the non-reciprocating reference datum was found.

(3) Experimental evidence shows the mutually affected coupling effects between rib-associated flows and the centrifugal, inertial, pulsating and buoyancy forces on heat transfer. In this respect, it seems that the coupling between buoyancy and pulsating forces could be isolated from the effects of cross-stream Dean vortices. When the reciprocating buoyancy effect was present in isolation, it provided consistent heat transfer enhancement which could sometimes lead to heat transfer improvement relative to the non-reciprocating reference.

(4) By extrapolating the experimental data to the implied zero buoyancy condition, it has been possible,

to isolate the effect of pulsating and centripetal buoyancy on heat transfer over the inner and outer edges for the rib-affected reciprocating helical pipe flow. These zero buoyancy solutions seem to be independent of the location with respect to the reciprocating effect in terms of scaled Nusselt number, Nu/Nu_0. For pulsating force effect alone, the most severe heat transfer impediment took place at about a pulsating number of 0.24 under which condition the heat transfer levels could be reduced to about 53% of the non-reciprocating reference. Such heat transfer impediment has to be considered particularly when the method of surface enhancement was adopted in the reciprocating helical coils.

(5) The proposed correlation for the inner and outer edges permits the individual and combined effects of pulsating force and reciprocating buoyancy in the ribbed coils to be taken into account.

Acknowledgements

This work was financially supported by National Science Council, Taiwan, Republic of China, under grant numbers, NSC-89-2212-E-022-002. Four of our research students, namely, Wang Han-Tsung, Kuo, Ming Hui, Hsu, Yu-Chen and Yeh, C. I. are fully involved in our current research works and their participation is highly appreciated.

References

[1] A. Aeberli, Sulzer RTA 60C – the new-generation two-stroke propulsion engine, Marine News, WARTSILA NSD CORPORATION (2) (1999) 4–6.
[2] S.W. Chang, Heat transfer of orthogonal-mode reciprocating tube fitted with twisted-tape, J. Exp. Heat Transfer 13 (2000) 61–86.
[3] S.W. Chang, L.M. Su, T.L. Yang, C.C. Hwang, An experimental study of heat transfer in reciprocating square duct fitted with ribs skewed to the flow, ASME J. Heat Transfer 121 (1999) 232–236.
[4] S.W. Chang, L.M. Su, C.C. Hwang, T.L. Yang, Heat transfer in a reciprocating duct fitted with transverse ribs, J. Exp. Heat Transfer 12 (1999) 95–115.
[5] S.W. Chang, L.M. Su, Influence of reciprocating motion on heat transfer inside ribbed duct with application to piston cooling in marine diesel engine, J. Ship Res. 41 (4) (1997) 332–339.
[6] A. Okajima, T. Matsumoto, S. Kimura, Aerodynamic characteristics of flat plates with various angles of attack in oscillatory flow, JSME Int. J. Ser. B 41 (1) (1998) 214–220.
[7] W.H. Lyne, Unsteady viscous flow in curved pipe, J. Fluid Mech. 45 (1971) 13–31.
[8] R. Zalosh, W.G. Nelson, Pulsating flow in a curved tube, J. Fluid Mech. 59 (1973) 693–705.
[9] H.A. Simon, M.H. Chang, J.C.F. Chow, Heat transfer in curved tubes with pulsatile fully developed laminar flow, ASME J. Heat Transfer 99 (1977) 590–595.
[10] N.J. Rabadi, J.C.F. Chow, H.A. Simon, Heat transfer in curved tubes with pulsating flow, Int. J. Heat Mass Transfer 25 (1982) 195–203.
[11] C.C. Hamakiotes, S.A. Berger, Periodic flows through curved tubes: the effect of the frequency parameter, J. Fluid Mech. 210 (1990) 353–370.
[12] J.H. Chung, J.M. Hyun, Heat transfer from a fully-developed pulsating flow in curved pipes, Int. J. Heat Mass Transfer 37 (1994) 42–52.
[13] L. Zabielski, A.J. Mestel, Unsteady blood flow in a helically symmetric pipe, J. Fluid Mech. 370 (1998) 321–345.
[14] L. Guo, X. Chen, Z. Feng, B. Bai, Transient convective heat transfer in a helical coiled tube with pulsatile fully developed turbulent flow, Int. J. Heat Mass Transfer 41 (1998) 2867–2875.
[15] Editorial Board of ASME Journal of Heat Transfer, Journal of heat transfer policy on reporting uncertainties in experimental measurements and results, ASME J. Heat Transfer 115 (1993) 5–6.
[16] C.X. Lin, M.A. Ebadian, The effects of inlet turbulence on the development of fluid flow and heat transfer in a helically coiled pipe, Int. J. Heat Mass Transfer 42 (1999) 739–751.
[17] R.A. Seban, E.F. Mclaughlin, Heat transfer in tube coils with laminar and turbulent flows, Int. J. Heat Mass Transfer 6 (1963) 387–395.